

Exploring the Effect of the Number of Hydrogen Atoms on the Properties of Lanthanide Hydrides by DMFT

Yao Wei, Elena Chachkarova, Evgeny Plekhanov, Nicola Bonini, and Cedric Weber

King's College London, Theory and Simulation of Condensed Matter (TSCM), The Strand, London WC2R 2LS, UK

(Dated: April 1, 2022)

Lanthanide hydrogen-rich materials have long been considered as one of the candidates with high-temperature superconducting properties in condensed matter physics, and have been a popular topic of research. Attempts to investigate the effects of different compositions of lanthanide hydrogen-rich materials are ongoing, with predictions and experimental studies in recent years showing that substances such as LaH_{10} , CeH_9 , and LaH_{16} exhibit extremely high superconducting temperatures between 150–250 GPa. In particular, researchers have noted that, in those materials, a rise in the f orbit character at the Fermi level combined with the presence of hydrogen vibration modes at the same low energy scale will lead to an increase in the superconducting transition temperature. Here, we further elaborate on the effect of the ratios of lanthanide to hydrogen in these substances with the aim of bringing more clarity to the study of superhydrides in these extreme cases by comparing a variety of lanthanide hydrogen-rich materials with different ratios using the dynamical mean-field theory (DMFT) method, and provide ideas for later structural predictions and material property studies.

Keywords: superconductivity; elemental composition; high pressure; DMFT

I. INTRODUCTION

Recently, hydrogen-rich materials have attracted great attention as potential candidates for high-temperature superconductivity, which is referred to as the holy grail of condensed matter physics. Since hydride causes high-frequency vibrations of hydrogen atoms at high pressure, it leads to stronger electron-phonon coupling, making it a potential high-temperature superconducting material [1, 2]. Almost 90 years ago, theoretical physicists E. Wigner and H. B. Huntington predicted that hydrogen, the lightest element in nature, would be extremely likely to metalize in a high pressure environment [3]. An early study in the 1960s on metallic hydrogen found superconductivity at temperatures close to or even above room temperature, which suggests that T_c of molecular hydrogen under high pressure is about 100–240 K, and that T_c of atomic hydrogen can reach 300–350 K also under high pressure [4, 5]. However, it is currently still difficult to perform relevant experiments due to the stringent synthesis requirements and ultra-sensitivity of metallic hydrogen under high pressure [6, 7]. As a result of development of computational tools for predicting crystal structures and calculating properties of materials, ultra-high pressure generators have emerged. Nowadays, theoretical and experimental research on hydrogen-rich compounds covers binary hydride materials formed by almost all elements, which also includes the lanthanum-based high-temperature superconducting material LaH_{16} [8], as well as CeH_9 [9–11], CeH_{16} , and YbH_{10} [12, 13]. Research on these materials has found that binary lanthanide superconducting materials with high hydrogen content at high pressure are characterized by high symmetry and that they exhibit a space group structure of hexagonal and cubic crystal systems under 200–300 GPa. In addition to lanthanide superconducting materials, there are also

hydrogen-rich superconducting materials with yttrium elements, which are chemically similar to lanthanides and often classified as rare earth metals YH_6 , YH_9 , and YH_{10} [14, 15]. Among the transition elements, many actinide-related superconducting materials have also been found, such as AcH_{10} , AcH_{12} , AcH_{16} , and ThH_{9-10} [16–18].

Furthermore, some common metal elements have been found to form hydrogen-rich materials with superconducting properties, which include CaH_6 [19–22], MgH_6 [23], MgH_{12} [24], to name a few.

In addition to the hydrogen-rich superconducting materials containing metallic elements, hydrogen-rich materials with nonmetals have also attracted much attention. In recent research, Ranga P. Dias reported the superconductivity of a C-S-H system with a maximal superconducting transition temperature of 287.7 ± 1.2 K (approximately 15 degrees Celsius) at 267 ± 10 GPa [25]. Besides, it was predicted that T_c values of PbH_8 , SbH_4 , and AsH_8 would be 178 K, 150 K, and 100 K above 200 GPa, 350 GPa, and 150 GPa respectively, as covalent hydrogenates [26, 27].

It has been found that LaH_{10} with face-centered cubic structure is a good metal, forming high electron-density energy bands at the Fermi level. The finite occupancy of the La- $4f$ orbitals, which are successively pushed at the Fermi level as the external pressure increases [28], ensures a particularly high T_c in La-H systems. The localized La- $4f$ orbitals become more stable compared to the La- $3d$ and La- $5d$ orbitals due to the pressure of the external environment, which leads to new prominent quantum states originating from strong electronic correlations [28].

Therefore, in order to more accurately describe the properties and physical laws of hydrogen-rich high-temperature superconductors at high pressures, the quantitative theoretical calculations were used in our research. The interaction between the localized electrons and the strong lattice vibrations of the hydrogen atoms

facilitates superconductivity in these materials. A thorough description of the electrical properties is required for a precise analysis of this interaction, which brings notorious difficulties for f -systems correlation, as it requires that both mobile and localized electrons are treated on the same basis [29].

Here, we present a study of the superconducting properties of two members of lanthanum hydrates family LaH_{10} and LaH_{18} in order to learn the effect of the hydrogen content on T_c and to find out if the many-body corrections to the DFT results are equally important for lanthanides with different hydrogen content. We employ a practical first-principles computationally consistent platform that uses a many-body correction of electron spectral weights and then feeds back into T_c 's estimate. In the present work, we limit ourselves to the DMFT corrections of the electronic spectrum only.

This paper proves that many-body correction in f -orbital systems may lead to changes occurring in spectral weights on the order of an eV. Our research presents an assessment of the physical properties of two La-H systems for different quantities of hydrogen atoms, paying particular attention to the influence of related factors on the spectral properties. It was found that LaH_{10} and LaH_{18} have stable crystal structures at pressures up to 400 GPa, while LaH_{18} is unstable at lower pressure; hence, we focus this investigation on modeling the materials at 400 GPa, as our aim is to compare the correction validity for different hydrogen compositions.

II. DISCUSSION

Electron-phonon interactions are thought to be the origin of superconductivity in lanthanide hydrides. According to the Migdal–Eliashberg theory, there are four factors to define T_c : the characteristic phonon frequency ω_{log} , the electron-phonon coupling strength λ , the density of states at the Fermi level $N(\epsilon_F)$, and the Coulomb pseudopotential, μ^* . Density functional theory (DFT), which uses standard pseudo-potentials and exchange correlation functionals, e.g., PBE, to explain lattice dynamics, is universally considered to be correct. It is generally acknowledged that DFT struggles to describe systems possessing strong electronic correlations with strongly localized d and f shells, and the use of many-body corrections are necessary.

In the following analysis, we used DFT combined with DMFT. In order to capture the local paramagnetic moment in lanthanide elements, one has to correct for local charge and spin fluctuations captured by DMFT. Changes in the orbital character at the Fermi surface produced by spectral weight transfer linked to Hubbard f band splitting are accounted for using DMFT. In accordance to the Allen–Dynes formalism, this affects low-energy electron-electron scattering processes via transfer of phonon momentum, which will be indicated in the following section.

We compared the effect of different DMFT electronic charge self-consistency schemes. A comparison is shown in Figure 1 between (i) PBE DFT and (ii) DFT+DMFT with full charge self-consistent formalism (DFT+DMFT+CSC). According to our research, we found that the Eliashberg function, $\alpha^2F(\omega)$, was significantly influenced by the correlation effects, which is defined in Equation (2). We utilized the Koster–Slater interaction vertex for the La correlated manifold, with values of $U = 6$ eV and $J = 0.6$ eV. From Figure 4 we can conclude that the DFT+DMFT+CSC method enables an increase in the superconducting temperature, which confirms the large contribution of the many-body effect to the prediction of the superconducting temperature of lanthanide hydrides, and justifies the need for more detailed correction models.

We noted that for the higher composition of hydrogen, LaH_{18} , the correction to the critical temperature is less significant compared to the lower hydrogen composition case. Figure 1 shows that the latter has a few well determined peaks that are enhanced by the DMFT+CSC correction, whilst in the LaH_{18} case, the Eliashberg function has a more evenly spread character with lower height of the peaks. Consequently, for the many-body corrections, we obtained an approximately 18% correction to LaH_{10} critical temperature compared to just under 4% for LaH_{18} , as can be seen from Figure 4. Note that $U = 6$ eV and $J = 0.6$ eV are used in the following section of this paper.

As shown in Figure 2a, the La compound is represented by a two-band system in the absence of a long-range magnetic order in DFT calculation. DFT formalism uses a single Slater determinant model and consequently fails to capture any paramagnetic effects, with an associated magnetic multiplet (fluctuating magnetic moment). These effects usually cause a splitting of spectral features into satellites, as seen in Figure 2b,c, with a resulting enforcement of the f character at the Fermi level. We established that since sharp La features exist at the Fermi level, a greater degree of theoretical modeling is necessary to correctly reflect the superconducting characteristics. In the conducted analysis, for example, the one-shot (DFT+DMFT) and the full-charge self-consistent method (DFT+DMFT+CSC) generate a minor shift of the acute La feature at the Fermi level, which reduces the f character weight at the Fermi level.

According to our results, f orbitals seem to be particularly significant for the superconducting characteristics of rare-earth hydrates. However, the impact of the quantity of the atoms for hydrogen in hydrate with the same f -element is unknown. Hence, in addition to LaH_{10} , we also studied stable LaH_{18} structures at 400 GPa with the aim to distinguish any notable tendencies.

A comparison between Figure 3a–c shows that the one-shot (DFT+DMFT) and the full-charge self-consistent method (DFT+DMFT+CSC) barely change the $4f$ La spectral weight at the Fermi level. This leads to similar results for the superconducting temperature

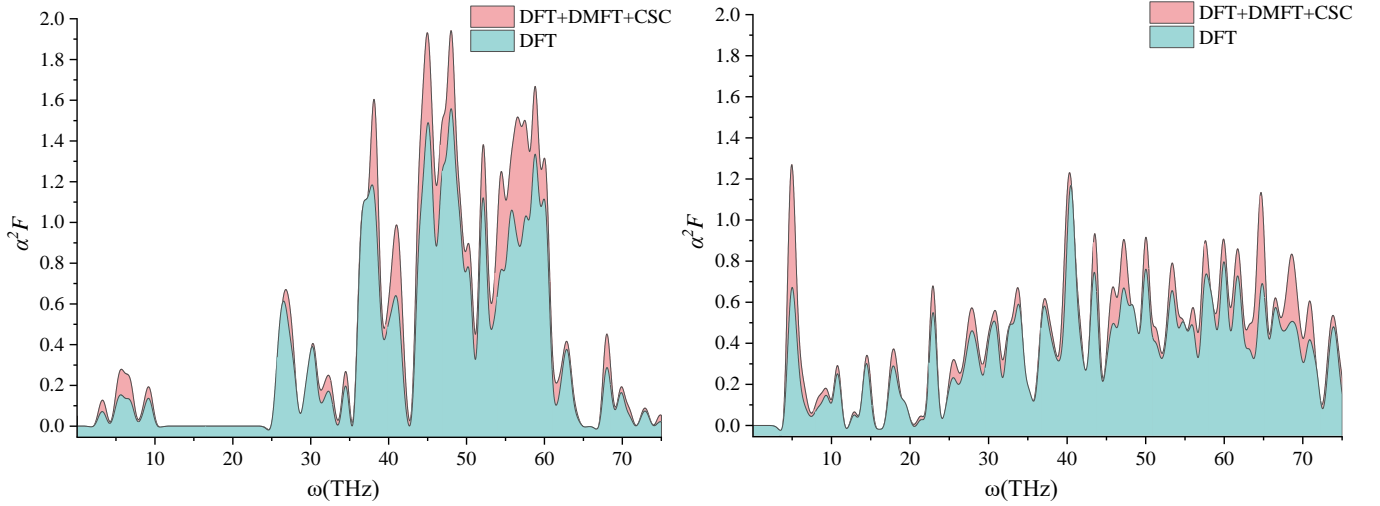


FIG. 1. Eliashberg function $\alpha^2 F(\omega)$ for (a) LaH_{10} and (b) LaH_{18} ; the spectral weight at the Fermi level is calculated with different extents of approximation: (i) DFT and (ii) with the full-charge self-consistent formalism (DFT+DMFT+CSC).

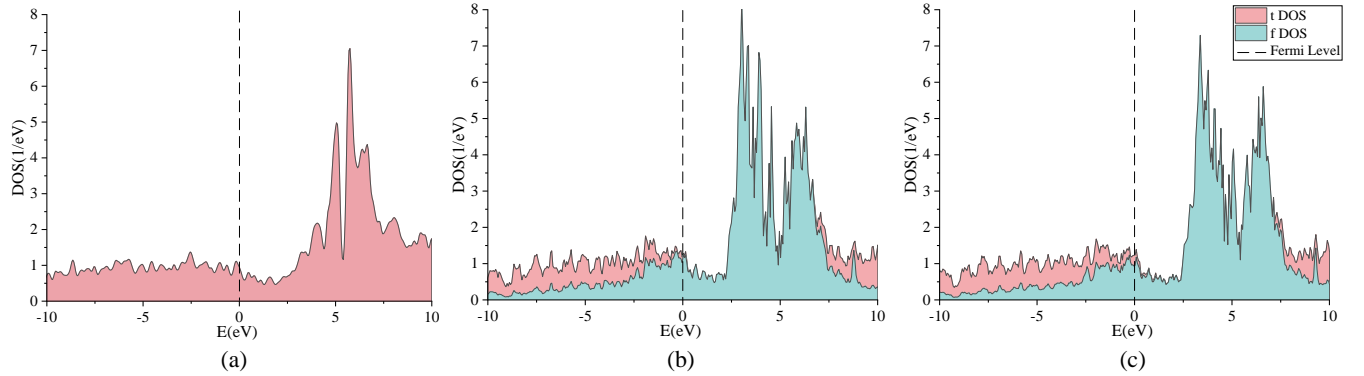


FIG. 2. (a) Density of states obtained by DFT calculations. $tDOS$ and $fDOS$ denote the density of states corresponding to the lattice and f impurity Green's function, respectively. In (b,c), we show the density of states, obtained by the one-shot DFT+DMFT and the full-charge self-consistent DFT+DMFT+CSC, respectively. All calculations were performed in the $\text{Fm}\bar{3}m$ phase of LaH_{10} at 400 GPa.

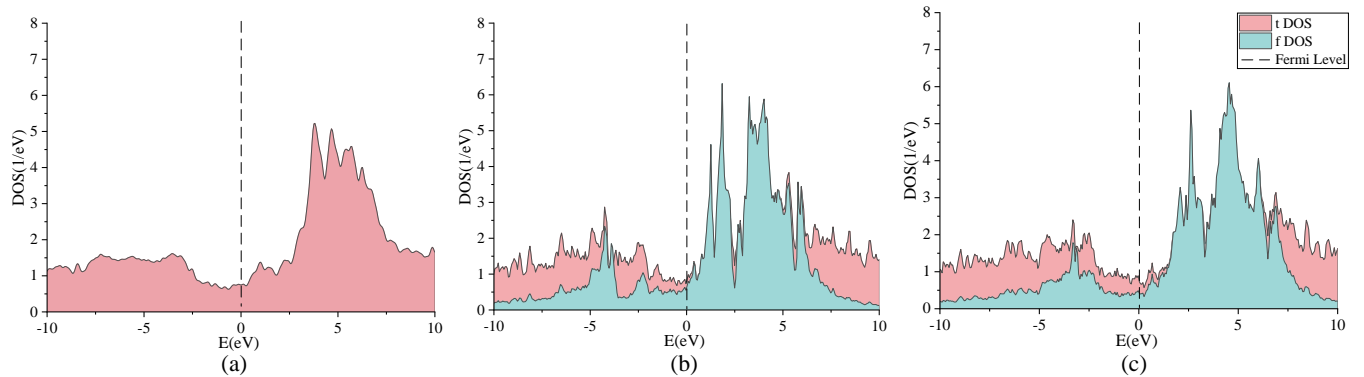


FIG. 3. (a) Density of states obtained by DFT calculations. $tDOS$ and $fDOS$ denote the density of states corresponding to the lattice and f impurity Green's function, respectively. In (b,c), we show the density of states, obtained by the one-shot DFT+DMFT and the full-charge self-consistent DFT+DMFT+CSC, respectively. All calculations were performed in the $\text{Fm}\bar{3}m$ phase of LaH_{18} at 400 GPa.

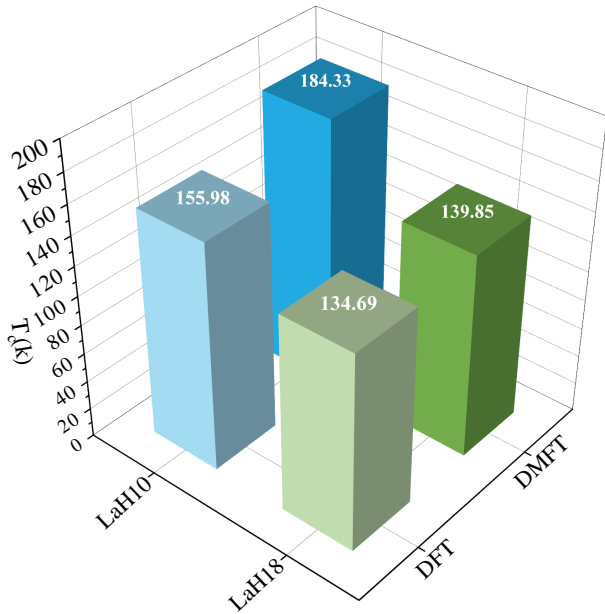


FIG. 4. The superconducting temperature T_c obtained by the Allen and Dynes formalism for LaH₁₀ and LaH₁₈ at 400 GPa. We obtained a theoretical estimate for LaH₁₀ of $T_c = 155.98$ K by DFT and $T_c = 184.33$ K by DMFT, as well as a theoretical estimate for LaH₁₈ of $T_c = 134.69$ K by DFT and $T_c = 139.85$ K by DMFT. We have used values of $U = 6$ eV and $J = 0.6$ eV. All calculations were performed in the Fm3m-LaH₁₀ and Fmmm-LaH₁₈ at 400 GPa.

of LaH₁₈ within DFT, one-shot DFT+DMFT, and DFT+DMFT+CSC approaches. By looking at Figures 2 and 3, it can be seen that the f orbital DOS modifications within DMFT with respect to DFT are different for different hydrogen content. For LaH₁₀, DFT significantly overestimates the $4f$ -La weight at the Fermi level, while for LaH₁₈, the $4f$ -La weight is low both in DFT and DMFT, leading to a lower T_c .

III. METHODS

Our theoretical approach is sketched in Figure 5. We provide a diagrammatic outline of the main elements of the proposed theoretical platform, as well as their interrelations. Our technique creates a modular structure for the screening of high-pressure materials.

Structural predictions. Crystal structure investigation by particle swarm optimization (CALYPSO) [30, 31], based on PSO algorithm [32, 33], provides stoichiometric compositions via Gibbs enthalpies for the equation of state and convex hull. The structure searches were carried out at 400 GPa with primitive cells of LaH₁₀ and LaH₁₈ for more than 600 structures.

Ab initio calculations. Structural optimization and

computations of enthalpy were performed using VASP code [34]. Electronic structures were calculated by QUANTUM ESPRESSO (QE) [35] code.

EPC calculations. We performed the electron-phonon coupling (EPC) calculation using QE with a kinetic energy cutoff of 90 Ry. In order to perform reliable calculation of the electron-phonon coupling in metallic systems, we have employed k -meshes of $2 \times 0.045 \text{ \AA}^{-1}$ for the electronic Brillouin zone integration and q -meshes of $2 \times 0.09 \text{ \AA}^{-1}$ for LaH₁₀ and LaH₁₈ compounds.

Methods. We combined the use of QE and CASTEP [36, 37] by using input file format conversion, pseudopotentials, and k -point grids. Core libraries for DMFT quantum embedding were used for the many-body corrections, which provided the total free energies, electronic densities, and Kohn-Sham levels occupancies [9, 38].

Norm-conserving pseudopotentials by OPIUM were adopted for describing the core electrons and their effects on the valence orbitals [39]. Reference electronic configurations of $5s^2 5p^6 5d^1 6s^2$ for the La atoms and $1s^1$ for the H atoms were used.

Post-processing. For estimating the superconducting transition temperature, T_c we used the Allen-Dynes modified McMillan equation [40]:

$$T_c = \frac{\omega_{\log}}{1.2} \exp \left[\frac{-1.04(1 + \lambda)}{\lambda - \mu^*(1 + 0.62\lambda)} \right] \quad (1)$$

where μ^* is the Coulomb pseudopotential. Formulas for the electron-phonon coupling strength λ and ω_{\log} were taken from Ref. [9]. In the post-processing stage, we have followed the procedure outlined by [9]; the reader interested in the computation details could refer to this paper for more exhaustive explanations of the steps, equations, and definitions of the relevant terms. Below, we quote the main equations that we used in our calculations of T_c .

The Allen-Dynes analysis models the Eliashberg function $\alpha^2 F(\omega)$ as a sum at the Fermi level over all scattering processes, mediated by phonon momentum transfer [41]:

$$\alpha^2 F(\omega) = N(\epsilon_F) \frac{\sum_{\mathbf{k}_1, \mathbf{k}_2} |M_{\mathbf{k}_1, \mathbf{k}_2}|^2 \delta(\epsilon_{\mathbf{k}_2}) \delta(\epsilon_{\mathbf{k}_1}) \delta(\omega - \omega_{\mathbf{q}\nu})}{\sum_{\mathbf{k}_1, \mathbf{k}_2} \delta(\epsilon_{\mathbf{k}_1}) \delta(\epsilon_{\mathbf{k}_2})} \quad (2)$$

where $N(\epsilon_F)$ is the DOS at Fermi level, $\omega_{\mathbf{q}\nu}$ is the phonon spectrum of a branch ν at momentum $\mathbf{q} = \mathbf{k}_2 - \mathbf{k}_1$, $\epsilon_{\mathbf{k}_1}$ and $\epsilon_{\mathbf{k}_2}$ are electronic band energies, referred to the Fermi level, while $M_{\mathbf{k}_1, \mathbf{k}_2}$ are the electron-phonon coupling matrix elements. When many-body corrections are taken into account, there is a shift of the spectral character at the Fermi level. Furthermore, the electronic correlations lead to a mass enhancement and induce a finite lifetime, due to incoherence. Following onto the DMFT scissors, the DFT bands are supplied with the renormal-

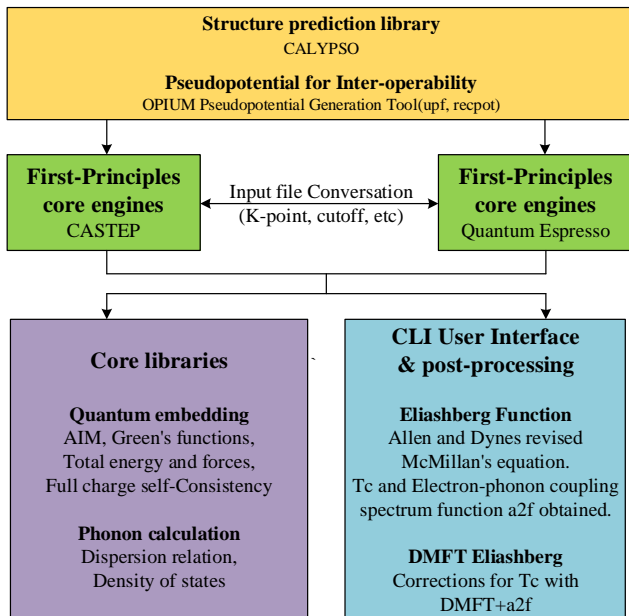


FIG. 5. **Schematic of the workflow for DFT+DMFT interfaced with Allen-Dynes.** Overview of the main modules of the theoretical platform and its interrelations. Firstly, structures are predicted by crystal structure analysis by particle swarm optimization (CALYPSO), and the pseudopotentials are generated with OPIUM. The underlying core engines are CASTEP and QE DFT software. We have used format conversion of input files, pseudo-potentials and \mathbf{k} -point grids to insure interoperability between QE and CASTEP. Core libraries are employed to provide the many-body corrections, via quantum embedding, which, in turn, provides corrected forces and energies. In post-processing, we used the *DMFT+a2f* approach to obtain values for the Eliashberg function and superconducting temperature T_c . Finally, data is archived for future usage using HDF5.

ized DMFT spectral density:

$$\alpha^2 F(\omega) = \mathcal{A}_{tot} \frac{\sum_{\mathbf{k}_1, \mathbf{k}_2} |M_{\mathbf{k}_1, \mathbf{k}_2}|^2 \delta(\omega - \omega_{\mathbf{q}\nu}) \mathcal{A}(\mathbf{k}_1) \mathcal{A}(\mathbf{k}_2)}{\sum_{\mathbf{k}_1, \mathbf{k}_2} \mathcal{A}(\mathbf{k}_1) \mathcal{A}(\mathbf{k}_2)}, \quad (3)$$

where \mathcal{A}_{tot} is the total and $\mathcal{A}(\mathbf{k})$ is the \mathbf{k} -momentum resolved spectral weight at the Fermi level. This method is indicated as *DMFT+a2f* in the model diagram. We would like to point out that, unlike the Allen–Dynes method using DFT eigenvalues, which suffers from the double-broadening issue, within our approach, the broadening is given by the finite lifetime from the many-body Green’s function and, therefore, our approach is free from the double broadening issue.

The DFT Kohn–Sham Eigenstates are employed in the derivation of the DMFT Green’s function in the DFT+DMFT quantum embedding approach [41]. The Anderson Impurity Model (AIM) is defined using atomic projectors and solved sequentially inside the Hubbard-I approximation. Furthermore, TRIQS open-source plat-

form [42] provides a wide range of quantum solvers through an interface to DMFT inside CASTEP. The Kohn–Sham potential is computed using the DMFT electronic density, which is generated from the DMFT occupancies, in the complete charge self-consistent technique (DFT+DMFT+CSC). Total energies and forces are determined using Green’s function and self-energy after DMFT convergence.

IV. CONCLUSIONS

We used many-body adjustments to predict the superconducting temperature in lanthanide hydrides and explored the significance of this model under different compositions with the same elements. To reestablish a consistent theoretical framework, the DMFT charge self-consistency method was utilized, including many-body corrections to the local charge density in first-principles calculations. Our methodology is free, flexible, and simple to implement, providing interaction of first-principles software with modular foundation. The software includes QE, CASTEP, and CASTEP+DMFT.

We found that an increase in the spectral weight of the f states at the Fermi level led to an increase in the estimated superconducting temperature. In this research, within the DFT+DMFT+CSC method, T_c was changed by 18% for LaH₁₀ and by 3% for LaH₁₈ at 400 GPa pressure. Furthermore, we discovered that the adjustment of the superconducting temperature of lanthanide materials within DFT+DMFT+CSC is more significant in symmetric structures and when the fraction of hydrogen elements is not excessively large.

DATA AVAILABILITY

The codes are available at url dmft.ai under the GPL 3.0 license.

AUTHOR CONTRIBUTION

Y.W. carried out the calculations. All authors wrote the paper. C.W. designed the research. All authors have read and agreed to the published version of the manuscript

FUNDING

Y.W. is supported by the China Scholarship Council. C.W., N.B., and E.P. are supported by Grant EP/R02992X/1 from the U.K. Engineering and Physical Sciences Research Council (EPSRC)

ACKNOWLEDGMENT

Y.W. is thankful to Dr. Ying Sun (Jilin University) for valuable discussions. This work was performed using resources provided by the ARCHER U.K. National Supercomputing Service and the Cambridge Service for Data Driven Discovery (CSD3) operated

by the University of Cambridge Research Computing Service (www.csd3.cam.ac.uk), provided by Dell EMC and Intel using Tier-2 funding from the Engineering and Physical Sciences Research Council (Capital Grant EP/P020259/1), and DiRAC funding from the Science and Technology Facilities Council (www.dirac.ac.uk)

-
- [1] McMahon, J.M.; Ceperley, D.M. High-temperature superconductivity in atomic metallic hydrogen. *Phys. Rev. B* **2011**, *84*, 144515.
- [2] Borinaga, M.; Errea, I.; Calandra, M.; Mauri, F.; Bergara, A. Anharmonic effects in atomic hydrogen: Superconductivity and lattice dynamical stability. *Phys. Rev. B* **2016**, *93*, 174308.
- [3] Wigner, E.; Huntington, H. On the possibility of a metallic modification of hydrogen. *J. Chem. Phys.* **1935**, *3*, 764.
- [4] Cudazzo, P.; Profeta, G.; Sanna, A.; Floris, A.; Continenza, A.; Massidda, S.; Gross, E. Ab initio description of high-temperature superconductivity in dense molecular hydrogen. *Phys. Rev. Lett.* **2008**, *100*, 257001.
- [5] McMahon, J.M.; Morales, M.A.; Pierleoni, C.; Ceperley, D.M. The properties of hydrogen and helium under extreme conditions. *Rev. Mod. Phys.* **2012**, *84*, 1607.
- [6] Erements, M.I.; Drozdov, A.P.; Kong, P.; Wang, H. Semimetallic molecular hydrogen at pressure above 350 gpa. *Nat. Phys.* **2019**, *15*, 1246.
- [7] Loubeyre, P.; Occelli, F.; Dumas, P. Synchrotron infrared spectroscopic evidence of the probable transition to metal hydrogen. *Nature* **2020**, *577*, 631.
- [8] Sun, W.; Kuang, X.; Keen, H.D.; Lu, C.; Hermann, A. Second group of high-pressure high-temperature lanthanide polyhydride superconductors. *Phys. Rev. B* **2020**, *102*, 144524.
- [9] Weber, C., Zhao, Z., Bonini, N., Plekhanov, E. & Others Computational materials discovery for lanthanide hydrides at high pressure for high temperature superconductivity. *Physical Review Research*. (2022)
- [10] Wang, C.; Liu, S.; Jeon, H.; Yi, S.; Bang, Y.; Cho, J.-H. Effect of hole doping on superconductivity in compressed CeH_9 at high pressures. *Phys. Rev. B* **2021**, *104*, L020504.
- [11] Li, B.; Miao, Z.; Ti, L.; Liu, S.; Chen, J.; Shi, Z.; Gregoryanz, E. Predicted high-temperature superconductivity in cerium hydrides at high pressures. *J. Appl. Phys.* **2019**, *126*, 235901.
- [12] Wei, Y.; Macheda, F.; Zhao, Z.; Tse, T.; Plekhanov, E.; Bonini, N.; Weber, C. High-temperature superconductivity in the lanthanide hydrides at extreme pressures. *Appl. Sci.* **2022**, *12*, 874.
- [13] Kruglov, I.A.; Semenov, D.V.; Song, H.; Szczesniak, R.; Wrona, I.A.; Akashi, R.; Esfahani, M.M.D.; Duan, D.; Cui, T.; Kvashnin, A.G.; et al. Superconductivity of LaH_{10} and LaH_{16} polyhydrides. *Phys. Rev. B* **2020**, *101*, 024508.
- [14] Kong, P.; Minkov, V.S.; Kuzovnikov, M.A.; Drozdov, A.P.; Besedin, S.P.; Mozaffari, S.; Balicas, L.; Balakirev, F.F.; Prakapenka, V.B.; Chariton, S.; et al. Superconductivity up to 243 K in the yttrium-hydrogen system under high pressure. *Nat. Commun.* **2021**, *12*, 1.
- [15] Struzhkin, V.; Li, B.; Ji, C.; Chen, X.-J.; Prakapenka, V.; Greenberg, E.; Troyan, I.; Gavriluk, A.; Mao, H.-K. Superconductivity in La and Y hydrides: Remaining questions to experiment and theory. *Matter Radiat. Extrem.* **2020**, *5*, 028201.
- [16] Semenov, D.V.; Kvashnin, A.G.; Kruglov, I.A.; Oganov, A.R. Actinium hydrides AcH_{10} , AcH_{12} , and AcH_{16} as high-temperature conventional superconductors. *J. Phys. Chem. Lett.* **2018**, *9*, 1920.
- [17] Semenov, D.V.; Kvashnin, A.G.; Ivanova, A.G.; Svitlyk, V.; Fominski, V.Y.; Sadakov, A.V.; Sobolevskiy, O.A.; Pudalov, V.M.; Troyan, I.A.; Oganov, A.R. Superconductivity at 161 K in thorium hydride ThH_{10} : Synthesis and properties. *Mater. Today* **2020**, *33*, 36.
- [18] Kvashnin, A.G.; Semenov, D.V.; Kruglov, I.A.; Wrona, I.A.; Oganov, A.R. High-temperature superconductivity in a Th-H system under pressure conditions. *Acs Appl. Mater. Interfaces* **2018**, *10*, 43809.
- [19] Wang, H.; John, S.T.; Tanaka, K.; Iitaka, T.; Ma, Y. Superconductive sodalite-like clathrate calcium hydride at high pressures. *Proc. Natl. Acad. Sci. USA* **2012**, *109*, 6463.
- [20] Shao, Z.; Duan, D.; Ma, Y.; Yu, H.; Song, H.; Xie, H.; Li, D.; Tian, F.; Liu, B.; Cui, T. Unique phase diagram and superconductivity of calcium hydrides at high pressures. *Inorg. Chem.* **2019**, *58*, 2558.
- [21] Ma, L.; Wang, K.; Xie, Y.; Yang, X.; Wang, Y.; Zhou, M.; Liu, H.; Yu, X.; Zhao, Y.; Wang, H.; et al. High- T_c superconductivity in clathrate calcium hydride CaH_6 . *ArXiv* **2021**, arXiv:2103.16282.
- [22] Li, Z.; He, X.; Zhang, C.; Zhang, S.; Feng, S.; Wang, X.; Yu, R.; Jin, C. Superconductivity above 200 K observed in superhydrides of calcium. *ArXiv* **2021**, arXiv:2103.16917.
- [23] Szczesniak, R.; Durajski, A. Superconductivity well above room temperature in compressed mgH_6 . *Front. Phys.* **2016**, *11*, 1.
- [24] Lonie, D.C.; Hooper, J.; Altintas, B.; Zurek, E. Metallization of magnesium polyhydrides under pressure. *Phys. Rev. B* **2013**, *87*, 054107.
- [25] Snider, E.; Dasenbrock-Gammon, N.; McBride, R.; Debessai, M.; Vindana, H.; Vencatasamy, K.; Lawler, K.V.; Salamat, A.; Dias, R.P. Room-temperature superconductivity in a carbonaceous sulfur hydride. *Nature* **2020**, *586*, 373.
- [26] Fu, Y.; Du, X.; Zhang, L.; Peng, F.; Zhang, M.; Pickard, C.J.; Needs, R.J.; Singh, D.J.; Zheng, W.; Ma, Y. High-pressure phase stability and superconductivity of pnictogen hydrides and chemical trends for compressed hydrides. *Chem. Mater.* **2016**, *28*, 1746.

- [27] Chen, B.; Conway, L.; Sun, W.; Kuang, X.; Lu, C.; Hermann, A. Phase stability and superconductivity of lead hydrides at high pressure. *Phys. Rev. B* **2021**, *103*, 035131.
- [28] Fedorov, A.; Laubschat, C.; Starke, K.; Weschke, E.; Barholz, K.-U.; Kaindl, G. Surface shift of the unoccupied 4f state in La metal. *Phys. Rev. Lett.* **1993**, *70*, 1719.
- [29] Pfeleiderer, C. Superconducting phases of f-electron compounds. *Rev. Mod. Phys.* **2009**, *81*, 1551.
- [30] Wang, Y.; Lv, J.; Zhu, L.; Ma, Y. Calypso: A method for crystal structure prediction. *Comput. Phys. Commun.* **2012**, *183*, 2063.
- [31] Wang, Y.; Lv, J.; Zhu, L.; Ma, Y. Crystal structure prediction via particle-swarm optimization. *Phys. Rev. B* **2010**, *82*, 094116.
- [32] Kennedy, J.; Eberhart, R. IEEE, particle swarm optimization. In Proceedings of the 1995 IEEE International Conference on Neural Networks Proceedings, Perth, Western Australia, 27 November–1 December 1995; Vols 1-61995.
- [33] Eberhart, R.; Kennedy, J. A new optimizer using particle swarm theory. In Proceedings of the Sixth International Symposium on Micro Machine and Human Science, Piscataway, NJ, USA, 4–6 October 1995; pp. 39–43.
- [34] Kresse, G.; Furthmüller, J. Efficient iterative schemes for ab initio total-energy calculations using a plane-wave basis set. *Phys. Rev. B* **1996**, *54*, 11169.
- [35] Giannozzi, P.; Baroni, S.; Bonini, N.; Calandra, M.; Car, R.; Cavazzoni, C.; Ceresoli, D.; Chiarotti, G.L.; Cococcioni, M.; Dabo, I.; et al. Quantum espresso: a modular and open-source software project for quantum simulations of materials. *J. Phys. Condens. Matter* **2009**, *21*, 395502.
- [36] Clark, S.J.; Segall, M.D.; Pickard, C.J.; Hasnip, P.J.; Probert, M.I.; Refson, K.; Payne, M.C. First principles methods using castep. *Zeitschrift für Kristallographie-Crystalline Materials* **2005**, *220*, 567.
- [37] Plekhanov, E.; Hasnip, P.; Sacksteder, V.; Probert, M.; Clark, S.J.; Refson, K.; Weber, C. Many-body renormalization of forces in f-electron materials. *Phys. Rev. B* **2018**, *98*, 075129.
- [38] Lee, H.; Plekhanov, E.; Blackburn, D.; Acharya, S.; Weber, C. The mott to kondo transition in diluted kondo superlattices. *Commun. Phys.* **2019**, *2*, 1.
- [39] Rappe, A.M.; Rabe, K.M.; Kaxiras, E.; Joannopoulos, J. Erratum: Optimized pseudopotentials [phys. rev. b 41, 1227 (1990)]. *Phys. Rev. B* **1991**, *44*, 13175.
- [40] Dynes, R. Mcmillan's equation and the T_c of superconductors. *Solid State Commun.* **1972**, *10*, 615.
- [41] Allen, P.B.; Dynes, R. Transition temperature of strongly-coupled superconductors reanalyzed. *Phys. Rev. B* **1975**, *12*, 905.
- [42] Parcollet, O.; Ferrero, M.; Ayrál, T.; Hafermann, H.; Krivenko, I.; Messio, L.; Seth, P. Triqs: A toolbox for research on interacting quantum systems.